

# Identification of the Operating Modes in Single-Phase DC Drives

Ahmet Kaymaz\*, Mehmet Akbaba, and Ali Akay


**Abstract**— In this study, operating modes of controlled single-phase rectifier-driven direct current (DC) drives were investigated. It was observed that the motor performance exhibited different behaviours depending on the combined interaction of the rectifier firing angle, motor parameters, motor load (or speed), supply voltage and frequency. It can be said that the voltage across the motor and the current through the motor take different waveforms in each of these different states, which are named drive operating modes in this study. Furthermore, analysis and simulations were conducted for two different types of drives: a) Single-phase fully controlled bridge rectifier drive (FCBRD) and b) Single-phase half-controlled bridge rectifier drive (HCBRD), including a freewheeling diode. As a result, the motor current waveform exhibits seven distinct operating modes, each performing different characteristics when driven by two types of rectifier circuits. On the other hand, the mathematical models of these seven modes were also presented in this study. The actual time variations of voltage across and current through the motor armature and the total harmonic distortion (THD) were presented through simulations for each mode using the obtained mathematical models in MATLAB.

**Index Terms**— DC drives, operating modes, performance analysis, phase-controlled rectifiers, total harmonic distortion.


## I. INTRODUCTION

DC MOTORS are widely used in many applications, such as in rolling mills [1], [2], [3], [4], the textile industry [5], [6], [7] and in some household appliances [8], [9], [10], [11]. In addition, they can be seen in robots, oil drilling facilities, rail transport and many other areas, such as the automotive industry [12], [13], [14], [15], [16]. Although the use of DC motors has decreased in recent years due to the ease of speed control


Ahmet Kaymaz, is with Department of Mechatronics Engineering, Karabuk University, Engineering Faculty, Karabuk, Turkey, (e-mail: [ahmetkaymaz@karabuk.edu.tr](mailto:ahmetkaymaz@karabuk.edu.tr)).

 <https://orcid.org/0000-0003-2262-1599>

Mehmet Akbaba, Professor Emeritus, (e-mail: [mehmetakbaba@karabuk.edu.tr](mailto:mehmetakbaba@karabuk.edu.tr)).

 <https://orcid.org/0000-0001-5013-091X>

Ali Akay, is with Department of Electrical-Electronics Engineering, Karabuk University, Engineering Faculty, Karabuk, Turkey, (e-mail: [ali.akay@karabuk.edu.tr](mailto:ali.akay@karabuk.edu.tr)).

 <https://orcid.org/0000-0001-7243-9395>

Manuscript received Apr 30, 2024; accepted Oct 7, 2024.  
DOI: [10.17694/bajece.1475619](https://doi.org/10.17694/bajece.1475619)

compared to AC motors, they are still intensively used in specific applications, as mentioned above [17], [18], [19].

Unbalanced operations and arcs due to commutation can cause severe damage to both the motor and the network when the DC motors are driven by the rectifiers [20], [21]. Moreover, motor performance can exhibit different behaviours depending on the combined interaction of the rectifier firing angle, motor parameters, motor load (or speed), supply voltage, and frequency. Therefore, it is necessary to accurately determine the current and voltage waveforms as well as total harmonic distribution (THD) for current or voltage that may arise when driving DC motors with rectifiers and to take the required precautions accordingly.

Although the analysis of controlled rectifier DC drives has been known for a long time [22], [23], [24], motor operating modes, which express the current-voltage waveforms that may arise depending on the firing angle of the rectifiers, have not been thoroughly investigated. Without detailed identification and analysis of the operating modes, detailed performance analysis and understanding of the operational behaviour of these drives cannot be considered completely. Therefore, in this study, the operating modes of the controlled single-phase rectifier-driven DC drives were thoroughly investigated and analyzed in detail. Thus, it was observed that the voltage across the motor and the current through the motor have different waveforms (seven distinct modes) in these operating modes.

While driving the same mechanical load, depending on the interaction between the parameters mentioned above, the drive may operate under different modes, i.e., in continuous current mode or one of the different discontinuous current modes [25], [26], [27]. Operation in different current modes exhibits various degrees of THD in motor armature current and supply current. High THD in the armature-current results in arc commutation and shortens the commutator life. Furthermore, high THD in the supply or armature current adversely affects the supply power factor and reduces the energy efficiency of the drive. Therefore, the main objective of this study is to identify various operating modes, address all the above essential issues through numerical simulations, and present the results in detail. Thus, this study can be a guide for engineers and researchers.

## II. IDENTIFICATION AND ANALYSIS OF THE OPERATING MODES

Two types of DC drives will be introduced in this part of the study. The first one is single-phase fully controlled bridge rectifier drives (FCBRD) that exhibit four distinct operating modes: Mode-I, Mode-II, Mode-III, and Mode-IV. The complete analysis and simulation of these modes are presented in detail. The second one is a single-phase half-controlled

bridge rectifier drive (HCBRD), including a freewheeling diode, which exhibits three distinct operating modes: Mode-V, Mode-VI and Mode-VII. This study also presents a detailed analysis and simulation of these modes. The performance of DC drives cannot be accurately evaluated without a complete understanding of the characteristics of these modes. On the other hand, the motor under study is a separately excited DC motor with a constant-rated excitation current. The motor specifications used for simulation are 240 V, 200 A, 45 kW, and 1800 rpm. Armature winding parameters and armature winding total inductance are also used as  $R_a = 0.143 \Omega$  and armature winding total inductance  $L_a = 0.02$  H. The supply voltage is rated at 220 V and frequency 50 Hz.

1. Modes of Operation of Single-Phase Fully Controlled Bridge Rectifier DC Drives (FCBRD)

As is known, in DC motors controlled with rectifiers, the supply voltage is generally preferred as the reference as the traditional method. However, it is worth noting that in the analysis below, the armature current will be considered as a reference, that is, the starting point of the armature current waves in each period. Moreover, in the following analysis, actual instantaneous armature current waveforms will be considered instead of average current waveforms, which are mostly considered in the related literature [18], [19], [25], [26], [27]. All quasi-state analyses assume that the motor speed, excitation current, and the motor's back-EMF are constant.

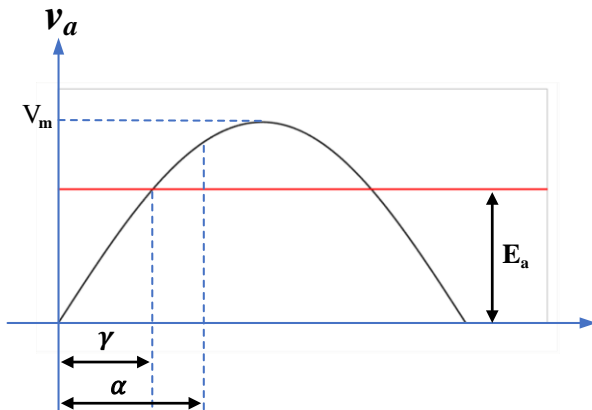


Fig. 1. Graphical representation of angles for  $\alpha$  and  $\gamma$ .

Simulation of each mode is performed in MATLAB using derived mathematical models. Thyristor firing angle ( $\alpha$ ) will be the main parameter throughout the analysis. Another critical

parameter is the angle, which corresponds to the time instant when supply voltage amplitude equals the motor back-EMF, indicated as  $\gamma$ , as shown in Fig. 1

Fig. 2 shows the schematic of the single-phase, fully controlled DC motor drive circuit. The input voltage of this system is expressed as  $v(t) = V_m \sin(\omega t)$ . The voltage appearing across the armature terminals, which is the output voltage of the rectifier, for a half cycle is given in Eq. (1).

$$v_a(\omega t) = V_m \sin(\omega t + \alpha) \quad (0 \leq \omega t \leq \pi) \quad (1)$$

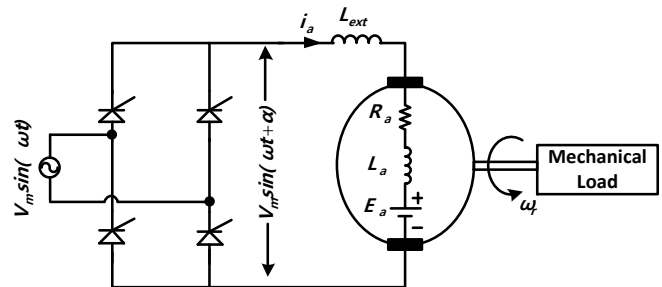


Fig. 2. Schematic of the single-phase fully controlled DC drive circuit.

The equation governing the motor armature loop is obtained as in Eq. (2), where  $L_{at} = L_a + L_{ext}$ .

$$V_m \sin(\omega t + \alpha) = R_a i_a + L_{at} \frac{di_a}{dt} + E_a, \quad (0 \leq \omega t \leq \pi) \quad (2)$$

Thus, the solution of Eq. (2) can be obtained as given in Eq. (3) where  $\Phi = \arctan(\omega L_{at}/R_a)$  and  $K$  is the integration constant which is calculated separately for each operating mode.

$$i_a(\omega t) = \frac{V_m}{Z} \sin(\omega t + \alpha - \Phi) + K e^{\frac{\omega t}{\tan \Phi}} - \frac{E_a}{R_a}, \quad (0 \leq \omega t \leq \pi) \quad (3)$$

Under constant excitation current and constant speed, the value of  $\alpha$  in Eq. (3) determines the current waveform and the motor's operating mode. The possible operating modes for the fully controlled bridge rectifier circuit (FCBRD), shown in Fig. 2, are given in Table 1.

As shown in Table 1, the operating mode can be labelled as Mode-I if the current is continuous. If the current is discontinuous, the operating mode can be one of Mode-II,

TABLE 1  
OPERATING MODES OF SINGLE-PHASE FULLY CONTROLLED DC DRIVE

$\alpha > \gamma$ or $\alpha < \gamma$	$\alpha > \gamma$	$\alpha < \gamma$	$\alpha < \gamma$
Continuous current mode	Discontinuous current mode	Discontinuous current mode for $I_{kr} > 0$	Discontinuous current mode for $I_{kr} < 0$
Mode-I	Mode-II	Mode-III	Mode-IV

Mode-III or Mode-IV. For discontinuous current, the mode is labelled as Mode-II if  $\alpha > \gamma$ , whereas it can be one of Mode-III or Mode-IV if  $\alpha < \gamma$ . Furthermore, Modes-III and Mode-IV are identified according to the critical current value,  $i_{kr}$ , which is the armature current value at the angle of  $(\pi - \gamma + \alpha)$ . Accordingly, if  $i_{kr} > 0$  ( $i_a(\pi - \gamma + \alpha) = i_{kr}$ ), then the operation mode is defined as Mode-III, and if  $i_{kr} \leq 0$ , the operating mode can be defined as Mode-IV.

#### A. Mode-I (Continuous Current Mode)

This operating mode is a continuous mode of the current in case of  $\alpha > \gamma$  or  $\alpha < \gamma$ . Thus,  $i_a(0) = i_a(\pi) > 0$  must be satisfied in Eq. (3) if the current is continuous. When this condition is considered, the integration constant  $K$  can be defined as in Eq. (4), and so the current is obtained as in Eq. (5). Thus, the average voltage expression can be written as in Eq. (6) and the average current expression is obtained as in Eq. (7).

$$K = \frac{2.V_m \cdot \sin(\alpha - \Phi)}{Z \cdot (1 - e^{(-\pi/\tan \Phi)})} \quad (4)$$

$$i_a(\omega t) = \frac{V_m}{Z} \left( \frac{\sin(\omega t + \alpha - \Phi)}{1 - e^{(-\pi/\tan \Phi)}} - \frac{2 \cdot \sin(\alpha - \Phi)}{1 - e^{(-\pi/\tan \Phi)}} \cdot e^{(-\omega t/\tan \Phi)} \right) - \frac{E_a}{R_a} \quad (5)$$

$$V_{avg} = \frac{1}{T} \int_0^T V(t) dt = \frac{2.V_m \cdot \cos(\alpha)}{\pi} \quad (6)$$

$$I_{avg} = (V_{avg} - E_a) / R_a \quad (7)$$

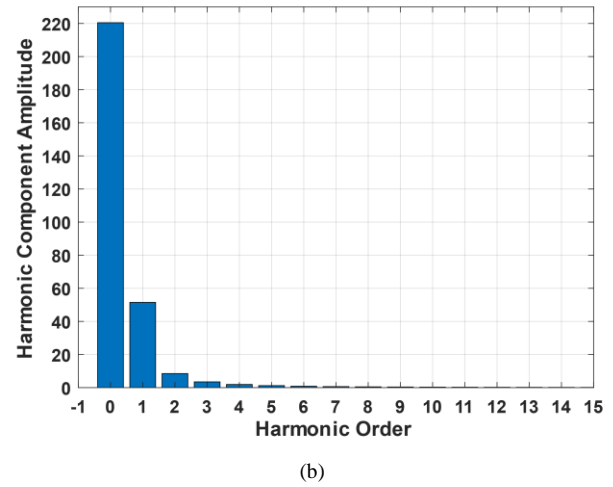
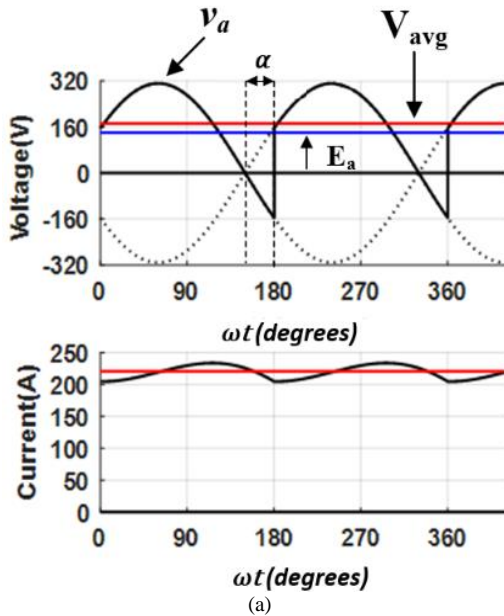


Fig. 3. Mode-I for the FCBRD circuit: a) current and voltage waveforms and b) harmonics in the current.

The voltage and current waveforms for Mode-I are plotted from the above analysis as in Fig. 3.a, and the harmonic content of the current is shown in Fig. 3.b. Thus, THD for current can be obtained as 6.42%, while the voltage ripple factor is calculated as 80.29% for  $\alpha = 30$ ,  $E_a = 140$  V and  $n = 1200$  rpm.

#### B. Mode-II (Discontinuous Current Mode for $\alpha > \gamma$ )

This operating mode is a current mode in which the current is discontinuous during  $\alpha > \gamma$ . In this mode, the boundary conditions, according to Eq. (3), must be as  $i_a(0) = i_a(\pi) = 0$ . And so, the current expression can be obtained as in Eq. (8) by considering boundary conditions. The expressions for the average voltage and current values can also be written as in Eq. (9) and Eq.(7), respectively.

$$i_a(\omega t) = \frac{V_m}{Z} \left( \frac{\sin(\omega t + \alpha - \Phi)}{1 - e^{(-\pi/\tan \Phi)}} + \frac{\sin(\alpha - \Phi)}{1 - e^{(-\pi/\tan \Phi)}} \cdot e^{-\omega t/\tan \Phi} \right) - \frac{E_a}{R_a} (1 - e^{-\omega t/\tan \Phi}) \quad (8)$$

$$V_{avg} = \frac{V_m}{\pi} (\cos(\alpha) - \cos(\theta + \alpha)) + E_a \cdot \left( \frac{\pi - \theta}{\pi} \right) \quad (9)$$

As a result, the current and voltage waveforms for Mode-II and current harmonics can be obtained as shown in Fig. 4. Thus, THD is obtained as 91.67%, and the ripple factor for armature voltage is 99.22% for  $\alpha = 60$ ,  $E_a = 140$  V and  $n = 1200$  rpm.

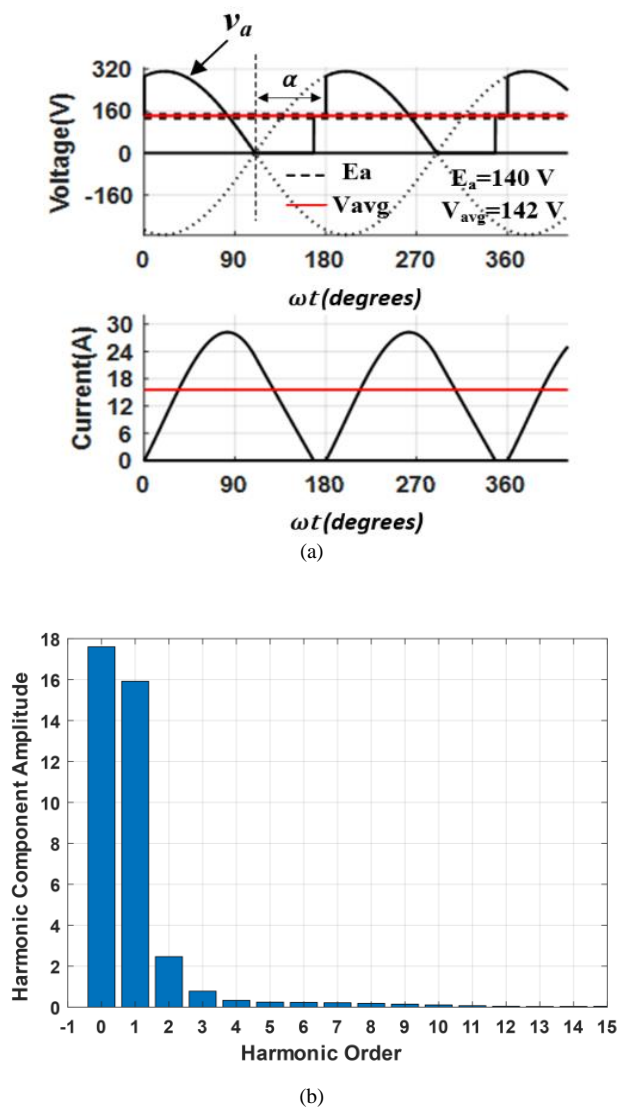


Fig. 4. Mode-II for the FCBRD circuit: a) current and voltage waveforms and b) harmonics in the current.

### C. Mode-III (Discontinuous Current for $\alpha < \gamma$ )

This operating mode is where the current is discontinuous for  $\alpha < \gamma$ . However, the operating mode could be Mode-III or Mode-IV in this situation. Therefore, the critical current at the time  $(\pi - \gamma + \alpha)$  should be determinants of distinguishing these two operating modes. If the armature current is zero at the critical time, the current remains at zero until the period is completed, whereas the armature voltage remains at back-EMF voltage ( $V_a = E_a$ ). However, during this time interval, if the current has not yet become zero, the voltage changes due to the thyristors triggered at the angle  $\alpha$ . Therefore, Mode-III is considered a different mode. In other words, if the condition  $i_{kr} = i_a(\pi - \gamma + \alpha) > 0$  is met, and the operating mode is labelled as Mode-III for the FCBRD circuit.

The current in Mode-III can be defined as a piecewise function using equation Eq. (3). Furthermore, for the interval of  $i_a < i_{kr}$ , the current is represented as  $i_{a1}$  and given by Eq. (10), while  $i_a \geq i_{kr}$ , the current is represented as  $i_{a2}$  and given by Eq. (11). According to the definition of Mode-III, the

boundary condition must be such that  $i_{a1}(0) = 0$ ,  $i_{a1}(\pi - \gamma + \alpha) = i_{a2}(0) = i_{kr} > 0$ . Thus, the average voltage and current expressions can be obtained in Eq. (12) and Eq. (7).

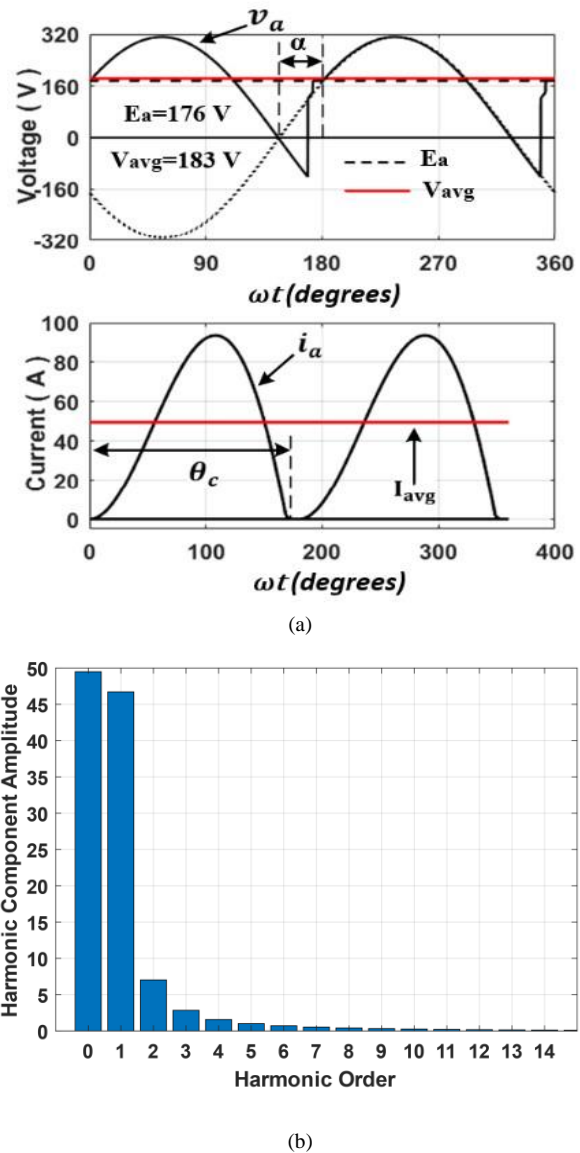


Fig. 5. Mode-III for the FCBRD circuit: a) current and voltage waveforms and b) harmonics in the current.

$$i_{a1}(\omega t) = \frac{V_m}{Z} (\sin(\omega t + \gamma - \Phi) + \sin(\gamma - \Phi) e^{-\omega t / \tan \Phi}) - \frac{E_a}{R_a} (1 - e^{-\omega t / \tan \Phi}) \quad (10)$$

$$i_{a2}(\omega t) = \frac{V_m}{Z} (\sin(\omega t + \alpha - \Phi) - 2 \sin(\alpha - \Phi) e^{-\omega t / \tan \Phi}) + \left( \frac{E_a}{R_a} - \frac{V_m}{Z} \sin(\gamma - \Phi) \right) e^{-(\omega t + \pi - \gamma + \alpha) / \tan \Phi} - \frac{E_a}{R_a} \quad (11)$$

$$V_{avg} = \frac{V_m}{\pi} (2 \cdot \cos(\alpha) + \cos(\gamma)) + \cos(\gamma + \theta) + E_a \cdot \left( \frac{\pi - \theta}{\pi} \right) \quad (12)$$

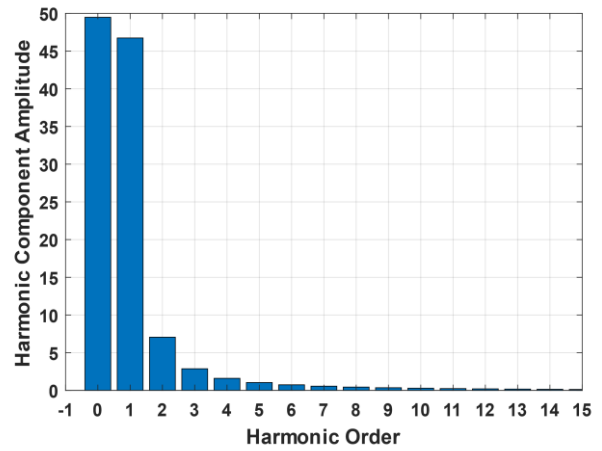
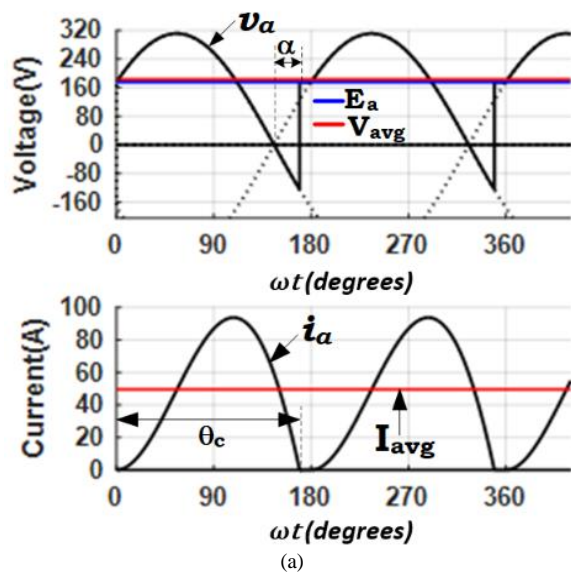
As a result, the current and voltage waveforms for Mode-III and the current harmonics are obtained, as shown in Fig. 5. Moreover, the THD is calculated as 95.72%, and the ripple factor for armature voltage is 67.16% for  $\alpha = 23$ ,  $E_a = 176$  V and  $n = 1500$  rpm.

**D. Mode-IV (Discontinuous Current Mode for  $\alpha < \gamma$ )**

This operating mode is the mode in which the current is discontinuous while  $\alpha < \gamma$ , such as Mode-III. However, the critical current is zero as opposed to Mode-III in this mode, that is,  $i_{kr} = i_a(\pi - \gamma + \alpha) = 0$ . In this case, mathematical analysis is similar to that of Mode-II. However, the current starts from  $\gamma$  instead of  $\alpha$ , unlike Mode-II. Therefore, according to the boundary conditions given by Eq. (3), the current equation is defined as in Eq. (13). Similar to the previous analyses, the average voltage and current expression can be obtained as in Eq. (14) and Eq. (7).

$$i_a(\omega t) = \frac{V_m}{Z} \sin(\omega t + \gamma - \Phi) + \left( \frac{E_a}{R_a} - \frac{V_m}{Z} \sin(\gamma - \Phi) \right) \cdot e^{-\omega t / \tan \Phi} - \frac{E_a}{R_a} \quad (13)$$

$$V_{avg} = \frac{V_m}{\pi} (\cos(\gamma) - \cos(\theta + \gamma)) + E_a \cdot \left( \frac{\pi - \theta}{\pi} \right) \quad (14)$$



(b)  
Fig. 6. Mode-IV for the FCBRD circuit: a) current and voltage waveforms and b) harmonics in the current.

Thus, the current and voltage waveforms and current harmonics are obtained, as shown in Fig. 6. Furthermore, the THD for the armature current and the ripple factor for the armature voltage can be calculated as 95.85% and 67.70%, respectively, for  $\alpha = 30$ ,  $E_a = 176$  V and  $n = 1500$  rpm.

**E. Transient Analysis for the Single-Phase FCBRD Circuit**

In this part of the study, the electromechanical equivalent circuit of the motor shown in Fig. 7 and the driver circuit given in Fig. 2 are used to perform the transient analysis. Eq. (2) is obtained from the drive circuit provided in Fig. 2. It is also possible to write the expression of  $E_a = k_T \omega_m$  assuming that the flux is constant ( $k_T$  is the torque constant). Thus, Eq. (15) can be written by leaving the derivative expression alone.

According to the circuit given in Fig. 7, Eq. (16) can be written and depends on the derivative of motor speed,  $T_L$  load torque and  $T$  electric moment produced by the motor, where  $J$  is the moment of inertia, and  $B$  is the friction coefficient. As a result, by taking into account Eq. (15) and Eq. (16) and using the Runge Kutta method, the behaviour of the armature current ( $i_a$ ) and the motor speed ( $\omega_m$ ) can be obtained as in Fig. 8 for continuous current mode and as in Fig. 9 for discontinuous current mode. The parameters are that  $\alpha = 30$ ,  $B=0.02$  N/(m/s) and  $J = 0.5$  kg.m<sup>2</sup> for continuous current mode, and  $\alpha = 70$  for discontinuous current mode.

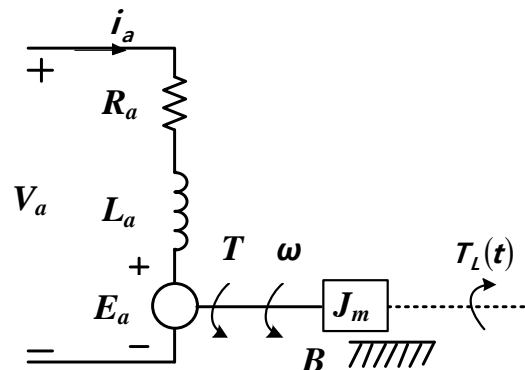


Fig. 7. Electromechanical equivalent circuit of a DC motor.

$$\frac{di_a}{dt} = \frac{1}{L_{at}}(V_a - R_a i_a - k_T \omega_m) \tag{15}$$

$$\frac{d\omega_m}{dt} = \frac{1}{J}(k_T \cdot i_a - T_L - B \cdot \omega_m) \tag{16}$$

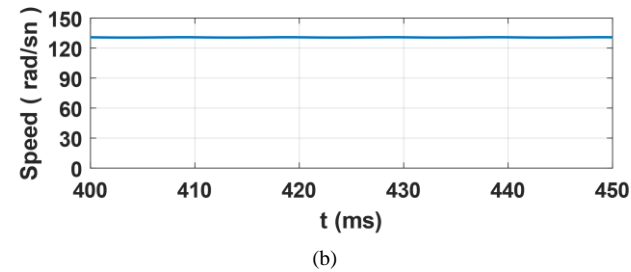
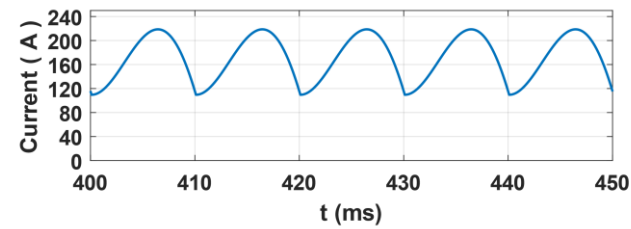
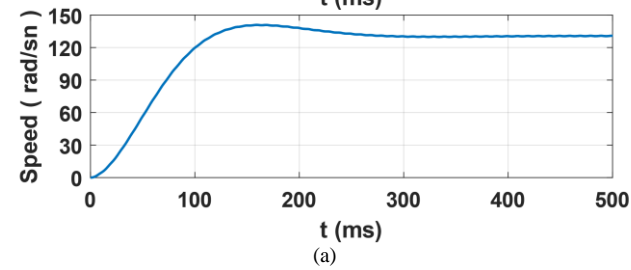
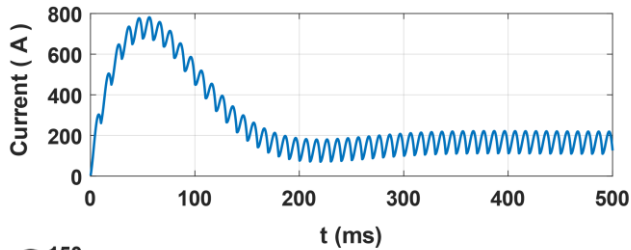


Fig. 8. Armature current and the motor speed for single-phase FCBRD circuit: a) current waveforms and motor speed for the total simulation time of 500 ms, and b) waveforms for steady-state.

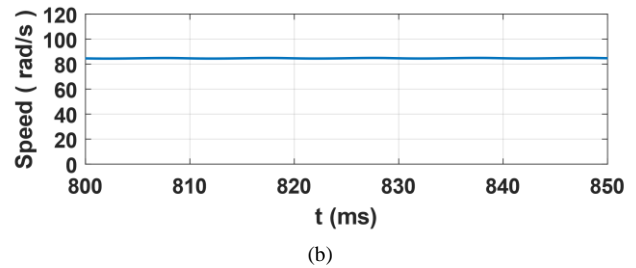
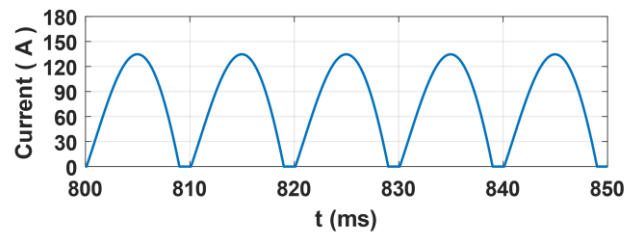
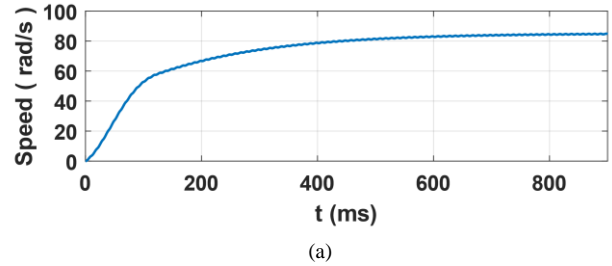
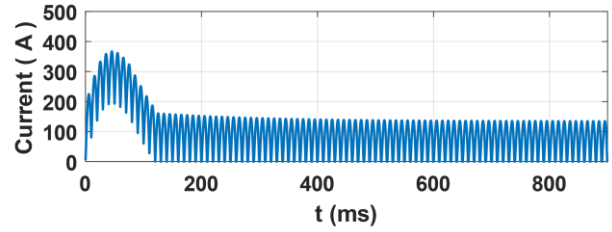


Fig. 8. Armature current and the motor speed at different values of the firing angle for the single-phase FCBRD circuit: a) waveforms for a total simulation time of 0.7 seconds, and b) waveforms for steady-state condition.

### 2. Operating Modes of Single-Phase Half-Controlled Bridge Rectifier Drive, Including a Freewheeling Diode

In the circuit given in Fig. 9, the first state is when the freewheeling diode is off position, and the second is when the freewheeling diode is on. If it is assumed that the commutation diode is ideal, in this case, Eq. (17) and Eq. (18) can be written for states I and II, respectively.

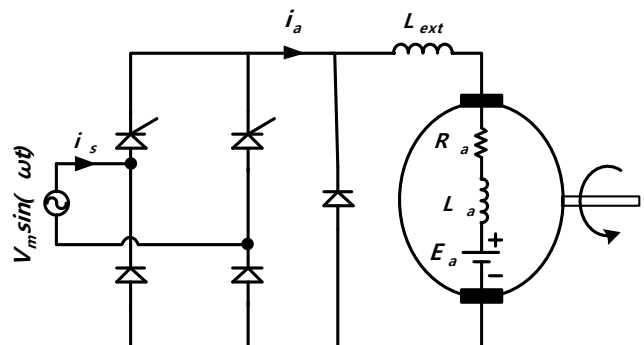


Fig. 9. Driving the DC motor with a single-phase HCBRD circuit.

State 1 :  $[0 \leq \omega t \leq (\pi - \alpha)]$ ;

$$i_{a1}(\omega t) = \frac{V_m}{Z} \sin(\omega t + \alpha - \Phi) + K_1 e^{-\omega t / \tan \phi} - \frac{E_a}{R_a} \tag{17}$$

State 2 :  $[(\pi - \alpha) \leq \omega t \leq \pi]$ ;

$$i_{a2}(\omega t) = K_2 e^{-(\omega t - \pi + \alpha) / \tan \phi} - \frac{E_a}{R_a} \tag{18}$$

Thus, Eq. (17) and Eq. (18) play critical roles in determining the operating modes for this circuit. In addition, it can be understood that different operating modes can occur due to the current and voltage waveforms changing according to the firing angle value. Therefore, the circuit shown in Fig. 9 is examined in three Modes: Mode-V, Mode-VI and Mode-VII.

Mode-V corresponds to the operating mode in which the current is continuous, while Mode-VI is the operating mode in which the current is discontinuous. On the other hand, Mode-VII represents the current mode in which the current drops to zero before the commutation diode becomes active, and therefore, the commutation diode never operates in this mode.

*A. Mode-V (Mode of the continuous current)*

According to the equations (17) and (18) obtained from the circuit given in Fig. 9, it is necessary to provide the condition of  $i_{a1}(\pi - \alpha) = i_{a2}(0)$  and  $i_{a1}(0) = i_{a2}(\alpha)$  so that the current is continuous. In this case, the currents for state I and II are given as in Eq.(19) and Eq.(20), respectively. On the other hand, the expressions corresponding to the average values of the voltage and the current can be obtained as in Eq. (21) and Eq. (7). As a result, the armature current and the voltage waveforms, as well as the FFT analysis of the armature current are depicted in Fig. 10. Thus, the THD for the current is found as 14.49%, and the ripple factor for voltage is 61.30% for  $\alpha = 30^\circ$ ,  $E_a = 140$  V and  $n = 1500$  rpm.

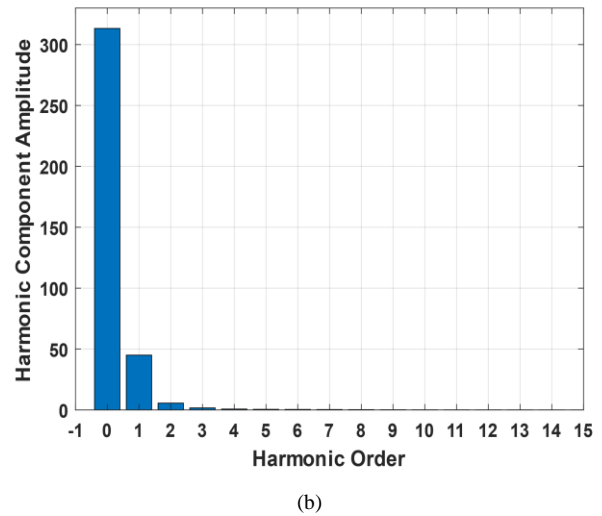
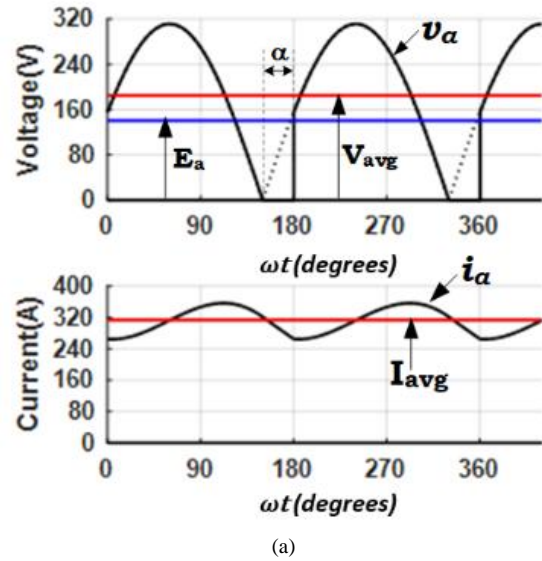


Fig. 10. Mode-V for the HCBRD circuit: a) current and voltage waveforms and b) THD analysis for the current.

$$i_{a1}(\omega t) = \frac{V_m}{Z} \left( \sin(\omega t + \alpha - \Phi) \cdot \left( \frac{\sin(\phi) e^{-\alpha / \tan \phi} - \sin(\alpha - \phi)}{1 - e^{-\pi / \tan \phi}} \right) \cdot e^{-\omega t / \tan \phi} \right) - \frac{E_a}{R_a} \tag{19}$$

$$i_{a2}(\omega t) = \frac{V_m}{Z} \left( \left( \frac{\sin(\phi) - \sin(\alpha - \phi) e^{-(\pi - \alpha) / \tan \phi}}{1 - e^{-\pi / \tan \phi}} \right) \cdot e^{-(\omega t - \pi + \alpha) / \tan \phi} \right) - \frac{E_a}{R_a} \tag{20}$$

$$V_{avg} = \frac{V_m}{\pi} (\cos(\alpha) + 1) \tag{21}$$

### B. Mode-VI (Discontinuous current mode)

In this operating mode, the current is discontinuous while the freewheeling diode is on. So, the conditions  $i_{a1}(0) = 0$  and  $i_{a1}(\pi - \alpha) = i_{a2}$  must be held. According to these boundary conditions, the currents for states I and II are obtained as in Eq.(22) and Eq. (23), respectively. Similarly, the average voltage and current can be found using Eq. (24) and (7). As a result, the current and the voltage waveforms and the THD analysis for the current are provided as in Fig. 11. Thus, the THD in the current is calculated as 93.32%, and the ripple factor for voltage is calculated as 82.41% for this operating mode that is  $\alpha = 70$ ,  $E_a = 140$  V and  $n = 1500$  rpm.

$$i_{a1}(\omega t) = \frac{V_m}{Z} \sin(\omega t + \alpha - \Phi) + \left( \frac{E_a}{R_a} - \frac{V_m}{Z} \sin(\alpha - \Phi) \right) \cdot e^{-\omega t / \tan \phi} - \frac{E_a}{R_a} \quad (22)$$

$$i_{a2}(\omega t) = \frac{V_m}{Z} \sin(\Phi) e^{-(\omega t - \pi + \alpha) / \tan \phi} + \left( \frac{E_a}{R_a} - \frac{V_m}{Z} \sin(\alpha - \Phi) \right) \cdot e^{-\omega t / \tan \phi} - \frac{E_a}{R_a} \quad (23)$$

$$V_{avg} = \frac{V_m}{\pi} (\cos(\alpha) + 1) + \frac{E_a}{\pi} (\pi - \theta) \quad (24)$$

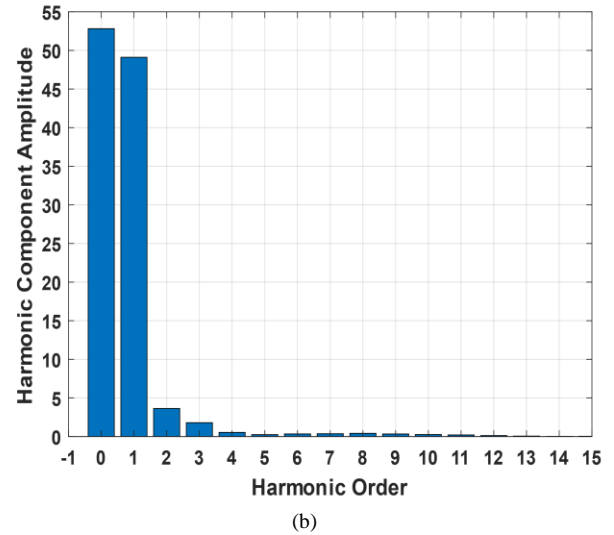
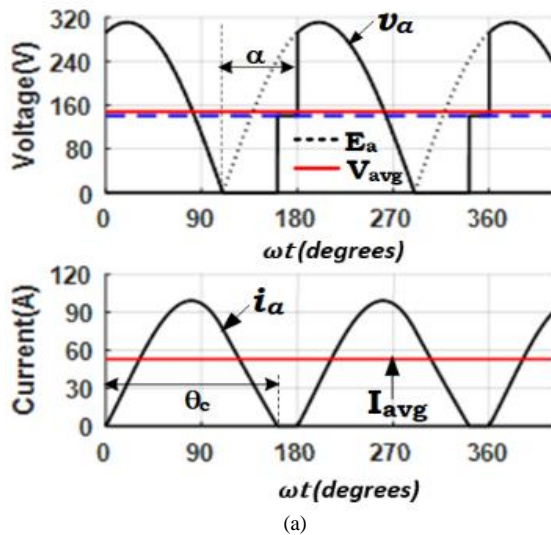


Fig. 11. Mode-VI for the HCBRD circuit: a) current and voltage waveforms and b) THD analysis for the current.

### C. Mode-VII (Discontinuous current mode)

The freewheeling diode is never activated in this operating mode because the armature current already drops to zero utilizing the thyristors in the current bridge circuit. Therefore, the condition  $i_{a1}(\theta) = i_{a1}(0) = 0$  can be written while the conduction angle is  $\theta < (\pi - \alpha)$ . According to these boundary conditions, the current is obtained as in Eq. (25) and Eq. (26). In this case, the average value of the voltage and the current will be as in Eq. (27) and Eq. (7), respectively.

$$i_{a1}(\omega t) = \frac{V_m}{Z} \sin(\omega t + \alpha - \Phi) + \left( \frac{E_a}{R_a} - \frac{V_m}{Z} \sin(\alpha - \Phi) \right) \cdot e^{-\omega t / \tan \phi} - \frac{E_a}{R_a} \quad (25)$$

$$i_{a2}(\omega t) = 0 \quad (26)$$

$$V_{avg} = \frac{V_m}{\pi} (\cos(\alpha) - \cos(\alpha + \theta)) + \frac{E_a}{\pi} (\pi - \theta) \quad (27)$$



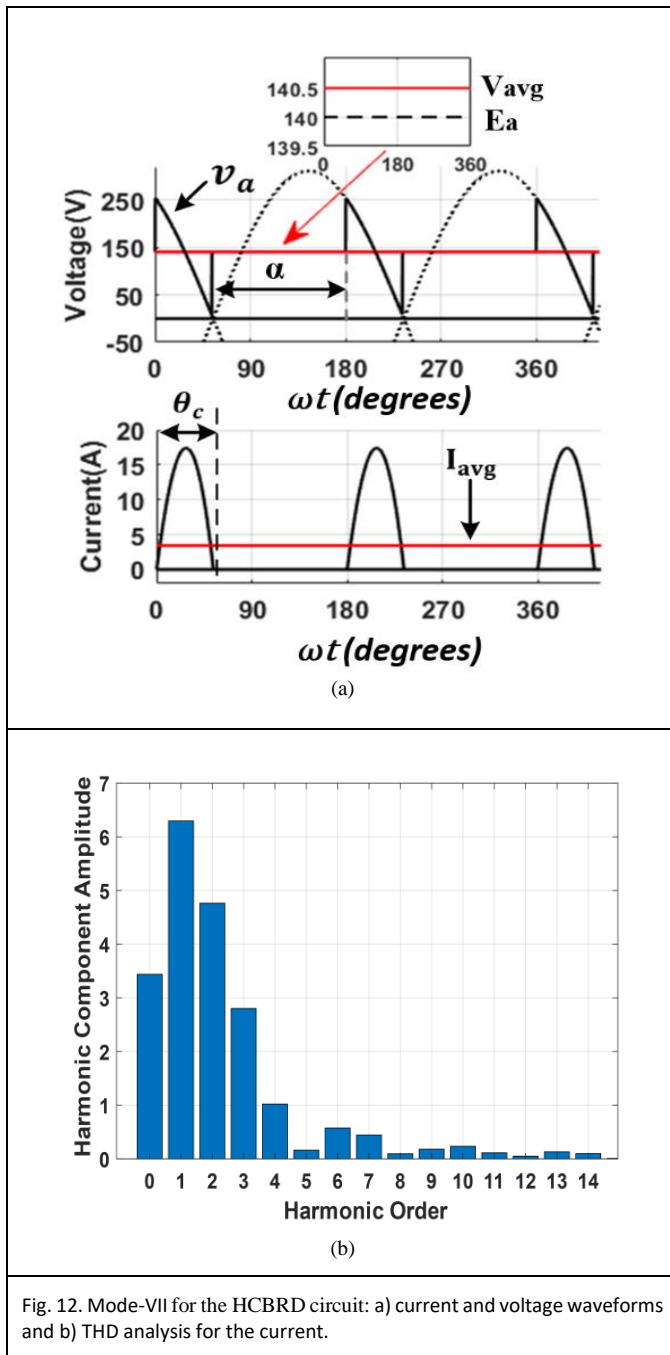


Fig. 12. Mode-VII for the HCBRD circuit: a) current and voltage waveforms and b) THD analysis for the current.

As in the other operating modes, the current and the voltage waveforms and the current harmonics are obtained by these equations as in Fig. 12. As a result, the total harmonic distortion in the current is calculated as 246.72%, and the ripple factor for the voltage is 28.09% for  $\alpha = 125$ ,  $E_a = 140$  V and  $n = 1500$  rpm in Mode-VII.

**D. Transient analysis for the single-phase HCBRD circuit**

The electromechanical equivalent circuit shown in Fig. 7 and the circuit shown in Fig. 9 are used to perform transient analysis of the HCBRD circuit. The differential equations for armature current for both states and the motor speed are given in Eq. (28), Eq. (29) and Eq. (30), respectively.

**State of [  $0 < \omega t < (\pi - a)$  ] ;**

$$\frac{di_a}{dt} = \frac{1}{L_{at}}(V_a - R_a \cdot i_a - k_T \omega_m) \tag{28}$$

**State of [  $(\pi - a) < \omega t < \pi$  ] ;**

$$\frac{di_a}{dt} = -\frac{1}{L_{at}}(R_a \cdot i_a + k_T \omega_m) \tag{29}$$

**State of [  $0 < \omega t < \pi$  ] ;**

$$\frac{d\omega_m}{dt} = \frac{1}{J}(k_T \cdot i_a - T_L - B \cdot \omega_m) \tag{30}$$

Simulation results for this analysis are depicted in Fig. 13 and Fig. 14, where the currents are continuous and discontinuous according to the firing angle. The parameters are that  $\alpha = 30$ ,  $B=0.02$  N/(m/s) and  $J = 0.5$  kg.m<sup>2</sup> for continuous current mode, and  $\alpha = 70$  for discontinuous current mode.

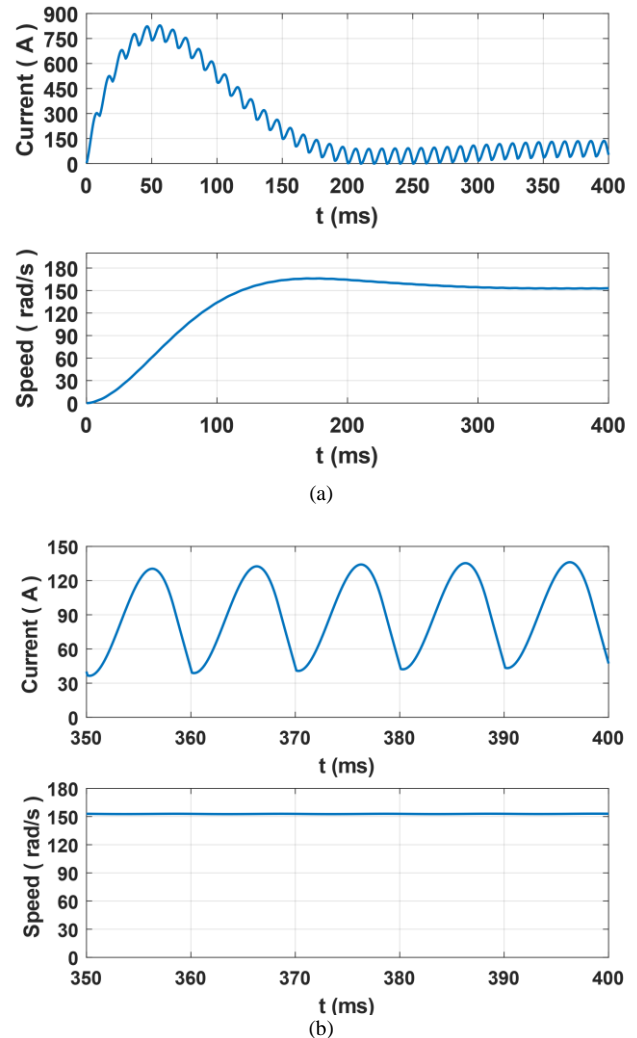


Fig. 13. Armature current and the motor speed for continuous current in the single-phase HCBRD circuit: a) waveforms for total simulation time of 400 ms, b) waveforms for steady-state condition.

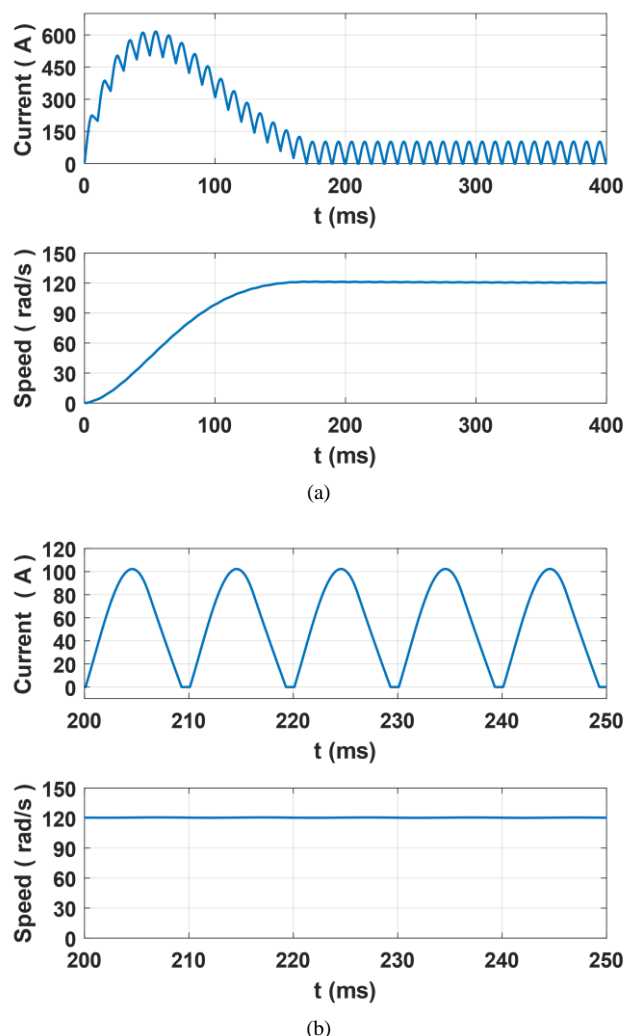


Fig. 14. Armature current and the motor speed for discontinuous current in the single-phase HCBRD circuit: a) waveforms for total simulation time of 400 ms, b) waveforms for steady-state condition.

### III. CONCLUSION

The operating modes that can occur as a result of driving DC motors with two different drive circuits were investigated in this study. Thus, seven operation modes were determined for two driver circuits consisting of single-phase fully-controlled and half-controlled bridge rectifier circuits. Analyses were made by analytically determining the current and voltage equations, as well as average current and average voltage equations for each operating mode. In addition, Fourier analysis of the current waveforms obtained for each operation mode was performed to determine the harmonic content of the current. The ripple factor of armature voltage was also calculated. On the other hand, transient analyses of armature current and motor speed were performed for each driver circuit, and waveforms were provided for these analyses. As a result, it is shown that there is one continuous current mode for both circuits, as well as three discontinuous current modes for the FCBRD circuit and two discontinuous current modes for the HCBRD circuit. Furthermore, it is shown that in some discontinuous modes, the peak armature current is much higher than the average current

value, resulting in high THD, which causes fast commutator deterioration. This behaviour is crucial for utilities.

TABLE 2.  
COMPARISON OF RIPPLE FACTOR AND THD VALUES

<i>FOR FCBRD CIRCUIT</i>				
<i>Operating Mode</i>	<i>Mode-I</i>	<i>Mode-II</i>	<i>Mode-III</i>	<i>Mode-IV</i>
<b>THD (%)</b>	6.42	91.67	95.72	95.85
<b>RF (%)</b>	80.29	99.22	67.16	67.70
<i>FOR HCBRD CIRCUIT</i>				
<i>Operating Mode</i>	<i>Mode-V</i>	<i>Mode-VI</i>	<i>Mode-VII</i>	
<b>THD (%)</b>	14.49	93.32	246.72	
<b>RF (%)</b>	61.30	82.41	28.09	

THD and RF of all modes are summarised in Table 2. In general, THD and RF do not show the same trend. From the supply and motor commutator life point of view, the THD is more critical than the RF. THD is better in continuous modes, i.e., Mode I and Mode V. Therefore, it is always better to operate the motor in continuous current mode, and it is always better to add more external inductance to the armature circuit to force the mode towards continuous current mode. However, more external inductance adds to the drive cost and more jule loss due to the resistance of the external inductance. Modes of operation depend on the load level. Lighter loads cause the motor to operate in one of the discontinuous current modes. Therefore, adding more external inductance can not always ensure continuous operation. Also, comparing discontinuous modes is not very meaningful as the load level changes and motor operation moves between the modes.

The role of freewheeling diodes in power electronic circuits is well known. It provides a path for the current in inductive circuits when the thyristors conducting current from the supply to the load have to stop conduction. Also, it prevents load voltage from going negative by providing a short circuit across the load and increases the average voltage across the load, as can be seen in Modes V-VII. Moreover, sharing current with the elements in the rectifier bridge reduces their ratings and results in relatively cheaper switching bridge devices. The relatively faster freewheeling diode can be preferable, and the rating can be closer to the rating of the devices in the bridge.

### ACKNOWLEDGE

This study consists of a part of the master's thesis conducted by the first author (Dr. Ahmet Kaymaz) under the supervision of Prof. Dr. Mehmet Akbaba.

### REFERENCES

- [1] S. I. Malafeev, A. A. Malafeeva, and V. I. Konyashin, "Correction of rolling mill mechatronic system to limit dynamic loads," *Russian Engineering Research*, vol. 38, pp. 431–433, 2018.
- [2] L. Fan and Y. Liu, "Fuzzy self-tuning PID control of the main drive system for four-high hot rolling mill," *Journal of Advanced Manufacturing Systems*, vol. 14, no. 01, pp. 11–22, 2015.
- [3] S. Liu, J. Liu, Z. Wu, and J. Li, "Bifurcation control for electromechanical coupling torsional vibration in rolling mill system driven by DC motor," *International Journal of Applied Electromagnetics and Mechanics*, vol. 50, no. 1, pp. 113–125, 2016.
- [4] J.-K. Ji and S.-K. Sul, "DSP-B based Self-Tuning IP Speed Controller with Load Torque Compensation for Rolling Mill DC Drive," 1995.

- [5] L. Dellinger, J. Nassour, and G. Cheng, "Dynamic model of an online programmable textile soft actuator," in 2023 IEEE International Conference on Soft Robotics (RoboSoft), IEEE, 2023, pp. 1–6.
- [6] J. C. Burgatti and R. A. Lacerda, "57mm Brushless DC Motor/BLDC Motor/Gear Motor for Textile Machinery CNC," *Revista da Escola de Enfermagem da USP*, vol. 43, no. 1, pp. 237–244, 2009.
- [7] V. S. Bosch, "Speed controlled single spindle drives for textile machines," in IECON'98. Proceedings of the 24th Annual Conference of the IEEE Industrial Electronics Society (Cat. No. 98CH36200), IEEE, 1998, pp. 2316–2320.
- [8] R. Raes and J. Schellekens, "A speed-controlled dc motor for a washing machine," *Philips Tech. Rev.*, vol. 34, no. 7, pp. 163–169, 1974.
- [9] U. Saleem and J. Kaźmierczak, "Building a Circular Economy Model for Managing Exploitation of Household Used Devices on the Example of Washing Machine Driven by DC Motor Along with Components," *Multidisciplinary Aspects of Production Engineering*, vol. 4, no. 1, pp. 309–316, 2021.
- [10] J.-W. Park, S.-H. Hwang, and J.-M. Kim, "Sensorless control of brushless DC motors with torque constant estimation for home appliances," *IEEE Trans Ind Appl*, vol. 48, no. 2, pp. 677–684, 2011.
- [11] R. B. Venkatesh and V. Sivaramkumar, "Design and fabrication of automatic dishwasher machine," *International Journal SSRG*, vol. 4, no. 3, pp. 26–31, 2017.
- [12] T. Shigemori and K. Sawa, "Characteristics of carbon and copper flat commutator on DC motor for automotive fuel pump," in Proceedings of the 50th IEEE Holm Conference on Electrical Contacts and the 22nd International Conference on Electrical Contacts Electrical Contacts, 2004., IEEE, 2004, pp. 523–527.
- [13] A. de la Guerra and L. Alvarez-Icaza, "Robust control of the brushless dc motor with variable torque load for automotive applications," *Electric Power Components and Systems*, vol. 48, no. 1–2, pp. 117–127, 2020.
- [14] R. Kahoul, Y. Azzouz, P. Marchal, and B. Mazari, "New behavioral modeling for DC motor armatures applied to automotive EMC characterization," *IEEE Trans Electromagn Compat*, vol. 52, no. 4, pp. 888–901, 2010.
- [15] H. Thieme, "Influence of automotive 42 V powernet on small PM DC motors," in IEMDC 2001. IEEE International Electric Machines and Drives Conference (Cat. No. 01EX485), IEEE, 2001, pp. 591–593.
- [16] W.-G. Shin and S.-H. Lee, "An analysis of the main factors on the wear of brushes for automotive small brush-type DC motor," *Journal of Mechanical Science and Technology*, vol. 24, pp. 37–41, 2010.
- [17] Z. Q. Zhu and J. H. Leong, "Analysis and mitigation of torsional vibration of PM brushless AC/DC drives with direct torque controller," *IEEE Trans Ind Appl*, vol. 48, no. 4, pp. 1296–1306, 2012.
- [18] M. Tariq and M. T. Iqbal, "Power quality improvement by using multi-pulse AC-DC converters for DC drives: Modeling, simulation and its digital implementation," *Journal of Electrical Systems and Information Technology*, vol. 1, no. 3, pp. 255–265, 2014.
- [19] G. C. Ioannidis et al., "AC-DC & DC-DC Converters for DC Motor Drives," in proceedings of the 2013 International Conference on Electronics and Communication Systems, 2013.
- [20] D. ÇELİK, "Performance Analysis of Three Levels Three Switches Vienna-Type Rectifier Based on Direct Power Control," *Balkan Journal of Electrical and Computer Engineering*, vol. 10, no. 2, pp. 170–177, Apr. 2022, doi: 10.17694/bajece.1072287.
- [21] A. KARAFİL and H. ÖZBAY, "Power Control of Single Phase Active Rectifier," *Balkan Journal of Electrical and Computer Engineering*, vol. 7, no. 3, pp. 332–336, Jul. 2019, doi: 10.17694/bajece.503207.
- [22] S.-J. Jeong and S.-H. Song, "Improvement of predictive current control performance using online parameter estimation in phase controlled rectifier," *IEEE Trans Power Electron*, vol. 22, no. 5, pp. 1820–1825, 2007.
- [23] P. Liutanakul, S. Pierfederici, and F. Meibody-Tabar, "Application of SMC with I/O feedback linearization to the control of the cascade controlled-rectifier/inverter-motor drive system with small dc-link capacitor," *IEEE Trans Power Electron*, vol. 23, no. 5, pp. 2489–2499, 2008.
- [24] N. Mohamed, T. Hamza, and G. Brahim, "Novel DTC induction machine drive improvement using controlled rectifier for DC voltage tuning," *International Journal of Power Electronics and Drive Systems (IJPEDS)*, vol. 10, no. 3, pp. 1223–1228, 2019.
- [25] J. H. Chen, K. T. Chau, and C. C. Chan, "Analysis of chaos in current-mode-controlled DC drive systems," *IEEE Transactions on Industrial Electronics*, vol. 47, no. 1, pp. 67–76, 2000.
- [26] M. Ilic and D. Maksimovic, "Digital average current-mode controller for DC–DC converters in physical vapor deposition applications," *IEEE Trans Power Electron*, vol. 23, no. 3, pp. 1428–1436, 2008.
- [27] B. Bryant and M. K. Kazimierzuk, "Modeling the closed-current loop of PWM boost DC-DC converters operating in CCM with peak current-mode control," *IEEE Transactions on Circuits and Systems I: Regular Papers*, vol. 52, no. 11, pp. 2404–2412, 2005.

## BIOGRAPHIES

**Ahmet Kaymaz** received the B.S. degree in Electrical and Electronics Engineering from the Pamukkale University, Denizli, in 2006. He also received his M.S. and Ph.D. degrees in Electrical and Electronics Engineering from the Karabuk University, Karabuk, Turkey, in 2015 and 2020, respectively. From 2010 to 2020, he was a Research



Assistant at Karabuk University. Since 2020, he has been an Asst. Prof. with the Karabuk University, Engineering Faculty, Department of Mechatronics Engineering.

**Mehmet Akbaba** received the M.S. degree from the İstanbul Technical University, Turkey in 1970 and the Ph.D. degree from the Strathclyde University, U.K. in 1977, all in Electrical Engineering. From 1977 to 1983 he was an assistant and associate professor with the Karadeniz Technical University, Turkey, from 1983 to 2012 he was an associate professor and full professor with the University of Bahrain, Bahrain, from 2012 to 2021 he was a full professor with the Karabuk University, Turkey. Currently, he is a professor emeritus. He has published over 100 papers and articles in refereed journals and Conference proceedings. His research interests include Power Electronics, Electrical Machines and Photovoltaics.



full professor with the University of Bahrain, Bahrain, from 2012 to 2021 he was a full professor with the Karabuk University, Turkey. Currently, he is a professor emeritus. He has published over 100 papers and articles in refereed journals and Conference proceedings. His research interests include Power Electronics, Electrical Machines and Photovoltaics.

**Ali Akay** received the B.S. degree in Electrical and Electronics Engineering from Erciyes University in 2010 and M.S. degree in Electrical and Electronics Engineering from Karabuk University in 2015. In 2021, he was awarded the Ph.D.



degree in the engineering department at University of Leicester, Leicester, UK. Since 2022, he has been an Assistant Professor with the Electrical and Electronics Engineering Department, at Karabük University. His research interests include fault-tolerant control of multiphase PM machines and control of three-phase and multiphase PM machines.